International Scholars Journals

African Journal of Wood Science and Forestry ISSN 2375-0979 Vol. 3 (9), pp. 198-210, September, 2015. Available online at www.internationalscholarsjournals.org © International Scholars Journals

Full length Research Paper

Depicting forest cover in Grand South of Cameroon: An analysis based on L-band PALSAR 50-m orthorectified imagery

Simon Njeudeng Tenku[1*], Xiangming Xiao[2] and Jinwei Dong[2]

[1]Institute of Agricultural Research for Development (IRAD), Regional Centre for Agricultural Research Nkolbisson (CRRANK), P.O Box 2123, Yaoundé Cameroon.
[2]Department of Microbiology and Plant Biology, and Centre for Spatial Analysis, University of Oklahoma, Norman, OK 73019, USA.

Accepted 14 August, 2015

Up-to-date information on forest cover is important for every country. Radar remote sensing technology has considerable potential to acquire cloud-free images in moist tropical forests due to frequent cloud cover. The objective of this study was to investigate the potential of Phased Array Type L-band SAR (PALSAR) imagery for forest cover mapping. 50-m orthorectified mosaic image of 2009 from L-band PALSAR was used for the study. Geo-referenced field photos were taken as ground truth data points and were organized to obtain regions of interest. K-means and decision tree classifications were carried out to discriminate forests from other land covers. Decision tree algorithm was more reliable than K-means and showed an overall accuracy assessment of 91.7 % and Kappa coefficient of 0.86. Decision tree estimated 24.4 million hectares of forests, that is, 12.5 % higher than 21 million hectares reported by ITTO in 2011. L-band PALSAR modelled backscatter output for the difference phase showed a grey tone pattern for forest cover similar to that of decision tree than to K-means; implying a spatial reliability for the modelled phase. Improved PALSAR-based forest cover mapping necessitates data coverage in both rainy and dry seasons.

Keywords: Remote sensing; forest cover mapping; PALSAR 50 m; field photo library; image texture.

INTRODUCTION

The Congo Basin is the second largest rainforest in the world and is recognized as one of the focused regions for climate change action mechanism (Justice et al., 2001; Zhang et al., 2005). With its more than 200 million hectares of contiguous rainforests, approximately 40 % of the population depend on these forests for their livelihoods and 80 % of these practise slash-and-burn agriculture (Bahuchet, 1995). The Grand South of Cameroon is within the Congo basin and harbors a very large portion of the Cameroon rainforest. The forest cover of Cameroon has been changing due to human activities related to slash and burn agriculture, logging, fuel wood collection, continual expansion of market-oriented agriculture and urban expansion (Essama-Nssah and Gockowski 2000; Mertens and Lambin 2000; Devers and Vande Weghe 2007; Epule et al. 2011). Two million hectares of this forest have been lost between 1980 and 1995 (Ndoye and Kaimowitz, 2000) and a report from Global Forest Watch in 2002 indicated an annual deforestation of 80 to 200 thousand hectares. In the year 2000, forest cover was estimated at 24.9 million ha (Wilkie and Laporte 2001). The state of the forest of the

*Corresponding Author: Email: sntenku2012@gmail.com

Congo Basin in 2008 reported forest cover of Cameroon at approximately 22.5 million ha (de Wasseige et al. 2009), while ITTO reported 21 million hectare in 2011.

The Grand South has in the past received much research interest due to its contribution to greenhouse gas emissions into the atmosphere from deforestation and forest degradation. It is to be mentioned here that the forest cover of Cameroon was estimated in 1985 through the use of extensive field surveys and aerial photography (Letouzey 1985). Extensive field survey for example involves a lot of man-power and the interpretation of aerial photography is usually susceptible to operator fatigue. In addition, photos from aerial photography have to be converted to digital format, which is required to get them to Geographical Information Systems. Although shortcomings from this approach are compensated for by the use of expert knowledge, the result is usually compromising and difficult to validate.

Technological advancement over the years has helped to improve data collection for forest cover estimates. Satellite remote sensing technology can collect information over an extended area of land in a relatively short time (Jensen 2007) and enables images to be collected in inaccessible areas. Remote sensing is efficient for forest cover mapping and is advancing at country specific level due to development of more efficient sensors to discriminate forest cover from other land covers.

Remote sensing operations using optical sensors have been carried out in the Grand South of Cameroon for forest cover estimate. The maps of forest cover were established from multi-temporal spectral classification with data obtained from Advanced Very High Resolution Radiometer (AVHRR) based on red and near infrared channels at 1.1 km spatial resolution (Laporte et al. 1998), Landsat TM (Thematic Mapper), ETM (Enhanced Thematic Mapper), and SPOT. Most of the acquisitions were done at coarse spatial resolution, which is good for global land coverage mapping, but disadvantageous at country-specific level (Belward and Lambin 1990; Mertens and Lambin 2000; Richards et al. 2000; Zhang et al. 2005). The forest of the Grand South is persistently covered with cloud and atmospheric impurities such as dust and smoke. Optical sensors are limited in acquiring cloud-free data and atmospheric impurities impede data collection. Radar remote sensing can overcome these problems (Lucas et al. 2004; Zhang et al. 2005; Ling et al. 2009; Ickowitz 2011). It has been shown that PALSAR-based forest cover map show large differences in forest cover estimates with GlobCover and FAO Forest Resource Assessment (FRA), but with very close estimate to that of MODIS (Dong et al. 2014).

Up-to-date and accurate forest cover maps are important to guide the government in making proper forest management plans. Radar sensors operate in different wavelength bands (X, C, L and P) to discriminate land covers (Kasischke et al. 1997). The research presented in this paper aims to provide a new estimate of forest cover for 2009 of the Grand South using the 2009 data acquisition of the Advance Land Observing Satellite (ALOS) Phased Array L-band Synthetic Aperture Radar (PALSAR). L-band ALOS PALSAR sensor uses microwave system which is capable to transmit electromagnetic energy that penetrates cloud and atmospheric impurities for data acquisition on the Earth (Henderson and Lewis, 1998; Jensen 2007). Long wavelength such as L-band (23.5 cm) has greater penetration into the forest. It is sensitive to large trees and big branches (Henderson and Lewis 1998) and less sensitive to less dense vegetated areas such as farmlands, banana, tea, rubber plantations and slash-and-burn areas (Jensen 2007; Santoro et al., 2009). Moisture content also affect microwave signals, which is important in depicting flooded areas under forest from pure water bodies and non-forest covers due to differences in grey tone levels (Saatchi and Soares 1997; Salas et al. 2002; Jensen 2007; Walker et al. 2010). PALSAR images show variations of pixel intensities called visual texture, which is characterized as the brightness or darkness of an image called tones. The spatial layout of the tones, usually grey-scale can practically be used to assess classifiers used in land cover classification (Tomppo et al. 1994; Soares et al. 1998; Tuceryan and Jain 1998; Sawaya et al. 2010).

The provision of up-to-date forest cover is part of Cameroon's initiative in support of REDD+ mission (reducing emissions from deforestation and forest degradation) as REDD+ addresses issues on forest cover extent to model carbon sinks and carbon emissions. The study wants to investigate if L-band PALSAR 50 m orthorectified image provides an alternative and reliable source for mapping forest cover. We applied simple classification scheme with four land covers: Forest, others (that is, unidentified land-use), cropland and water bodies and we used *a priori* information on grey tones distribution to support the classification accuracy. In addition, geo-referenced field photos of the study area were used to support radar imagery from L-band PALSAR to see the spatial richness of the different polarizations.

MATERIALS AND METHODS

The Study Area

The Grand South of Cameroon is located between latitudes 1° 88´–7° 22´ N and longitudes 8° 45´–16° 24´ E and characterized with altitudes that range from 0 m above sea level to above 4000 m on Mount Cameroon. It has an annual rainfall that ranges from 1600 mm to 3000 mm. The study area is characterized by a set of biophysical conditions that favour crop production, thus, the expansion of market-oriented plantations (palms, tea,

rubber and banana) (Hoyle and Levang 2012). We visited three regions of the Grand South (Southwest, Centre and South). These regions were considered because large amounts of the forest cover have been cleared for plantation agriculture.

PALSAR 50 m Orthorectified Mosaic Image Data

ALOS PALSAR 50 m Orthorectified Mosaic data were procured from JAXA PALSAR website (http://www.eorc.jaxa.jp/ALOS/en/kc_mosaic/kc_50_c_africa.htm#a13). They were created with images in the ascending path at an off-nadir angle of 34.3 degree and were resampled into the 50 m by 50 m mosaic with one composite per year. Data for the study area was acquired from June 12, 2009 to November 17, 2009. It implies data was acquired when there was rainfall and cloud cover in most part of the Grand South.

We used the PALSAR 50 m orthorectified mosaic product in 2009 with observational mode of Fine Beam Dual polarization (FBD). Due to variations in incident angle, topographic and geometric factors, the radar image, that is, its Digital Number (DN) values (amplitude values) were converted into normalized radar cross-section in decibel (dB) according to the formula from JAXA also known as sigma naught (σ^0) (Rosenqvist et al. 2007) and the parameters from the metadata of each file:

$$\sigma^0 (dB) = 10 \times log_{10}\{DN^2\} + CF \quad (1)$$

where σ^0 is the backscattering coefficient, *DN* is the digital number value of pixels in HH or HV and *CF* is the absolute calibration factor, which depends on the processing date and for Cameroon is -83. The model inputs for the PALSAR study were the following parameters: wavelength (L-band), polarizations (HH and HV) and incidence angle (34.3 degree). We further produced a ratio phase image (HH/HV) and a difference phase image (HH-HV) using band math in ENVI to see which of HH, HV, HH/HV and HH-HV model outputs agreed most to PALSAR data for forest cover mapping (Miettinen and Liew 2011).

Ground Reference Data

Field survey was done in March 2012 using the Casio digital camera (Casio Exilim 14.1 megapixels (EX-H20G)), which is equipped with a Hybrid-GPS system that combines a GPS receiver to take field photos of land covers. The GPS-enabled camera actually marks the location of each photo with a waypoint (longitude, latitude and altitude).

The ground truth geo-referenced photo data helped us to locate regions of forest cover, water bodies and non-forest. In this light, many photo waypoints were taken to explore the high resolution imagery provided by Google Earth. To avoid manually adding latitude and longitude coordinates on Google Earth to create polygons for our regions of interest, the geo-referenced photos were automatically uploaded to the Global Geo-Referenced Field Photo Library (www.eomf.ou.edu/photos/) managed by the Earth Observation and Modeling Facility of the University of Oklahoma (Xiao et al. 2011). Using the library we were able to download photo files related to forest cover, non-forest and water bodies as kml files. The kml files were exported to Google Earth to digitize the different land classes. It is to be mentioned again that the study focuses on forest cover, and we just did simple classifications for forest cover, non-forest (croplands and others), and water bodies as our regions of interest. The polygons for the different ROIs were then converted to shapefiles using ArcGIS and later exported to ENVI. The ROIs were randomly divided into two training ROIs and validation ROIs.

Land Cover Classification and Forest Identification

Figure 1 shows the schematic workflow for the forest cover mapping in this study. Though there are many classifications schemes, we considered Decision tree and K-means classifications for image classification, and we compared the results from these two algorithms using three regions of the Grand South in which the field survey was done. K-means classification is an unsupervised classification, which is powerful in spectral resolution and Decision tree uses a series of binary decisions to split objects into their right categories for each pixel, and to a level of certainty, it will solve the problem of neighbouring pixels most especially in complex and heterogeneous landscapes like the Grand South. For both classifiers, we used ENVI software to obtain the area occupied by the three land covers (forest, non-forest (croplands and others) and water bodies) for the South, Centre and South west regions.

Accuracy Evaluation of Forest Maps

A sample of 368 ROIs was developed, based on geo-referenced field photos we collected in 2012 using the high resolution images in the Google Earth; 162 ROI for the forest class, 150 ROI for non-forest and 56 ROI for water body. The samples were obtained in representative sites in all areas and were used for accuracy assessment. The representative sites were Bakingili forest reserve, the Bokwango forest site, the Campo-Ma'an buffer zone and the Mbalmayo forest reserve. They cover an area of 92 ha, 87 ha, 81,500 ha and 9,700 ha and the 368 ROIs and the number of pixels for each land cover is presented (Table 2). There are a total number of 7378 pixels, which was used to get the percentage of the area covered by our ROIs to the representative sites and the ratio is ~ 1.9 %.

Accuracy assessment was to determine to what degree ground truth data points agreed with the classification results of the PALSAR data from the Decision tree and K-

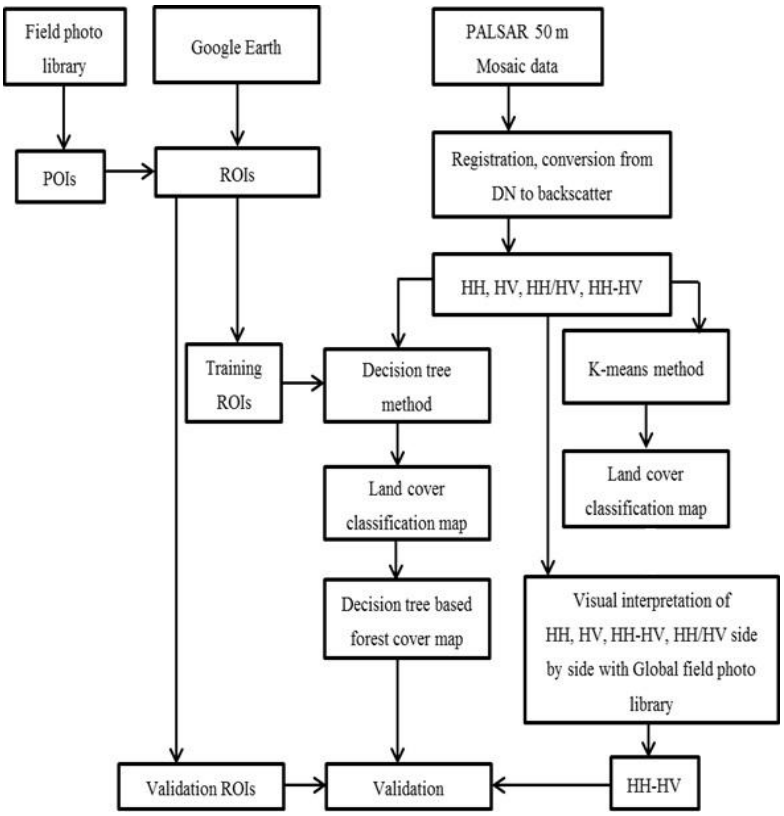

Figure 1. The workflow for mapping forest cover for the study area using PALSAR 50 m orthorectified mosaic imagery.

Table 1. Area estimates in hectare of forest (F), non-forest (NF) and water bodies (WB) from K-Mean and decision tree classifications for three regions within the Grand South where ground truth data were collected.

	Decision tree						K-means					
	South		Centre		South west		South		Centre		South west	
Land covers	Area (ha)	%	Area (ha)	%	Area (ha)	%	Area (ha)	%	Area (ha)	%	Area (ha)	%
Water bodies	1,500	0.04	11,100	0.16	3,700	0.15	6,100	0.13	38,770	0.56	20,050	0.81
Non-forest	445,200	9.31	1,427,200	20.58	609,100	24.59	142,900	2.99	659,260	9.50	274,200	11.07
Forest	4,329,400	90.65	5,498,100	79.26	1,863,800	75.26	4,627,100	96.88	6,238,370	89.94	2,182,300	88.12

means classifiers, but by examining the results of the three regions, we finally used a confusion matrix to continue analysis with Decision tree classifier for the various land covers (Table 2).

RESULTS

Land cover maps for the Grand South from decision tree and K-means classifiers

The spatial distribution of land cover classes for the Grand South is provided in Figure 2 belonging to K-means (a) and Decision tree (b) classifications. It is to be mentioned that croplands and others in the legend will represent the non-forest class in later part of the results. From the land cover maps, result from the Decision tree classification estimates 24.4 million hectares of forest cover for 2009, while that of the K-means classification estimates 27.3 million hectares of forest cover in 2009. The result from Decision tree is substantially lower by 13 % to 28 million hectare obtained by FAO in 2010 (FAO 2010) but larger (~ 16 %) than the 21 million hectare obtained by ITTO (ITTO 2011).

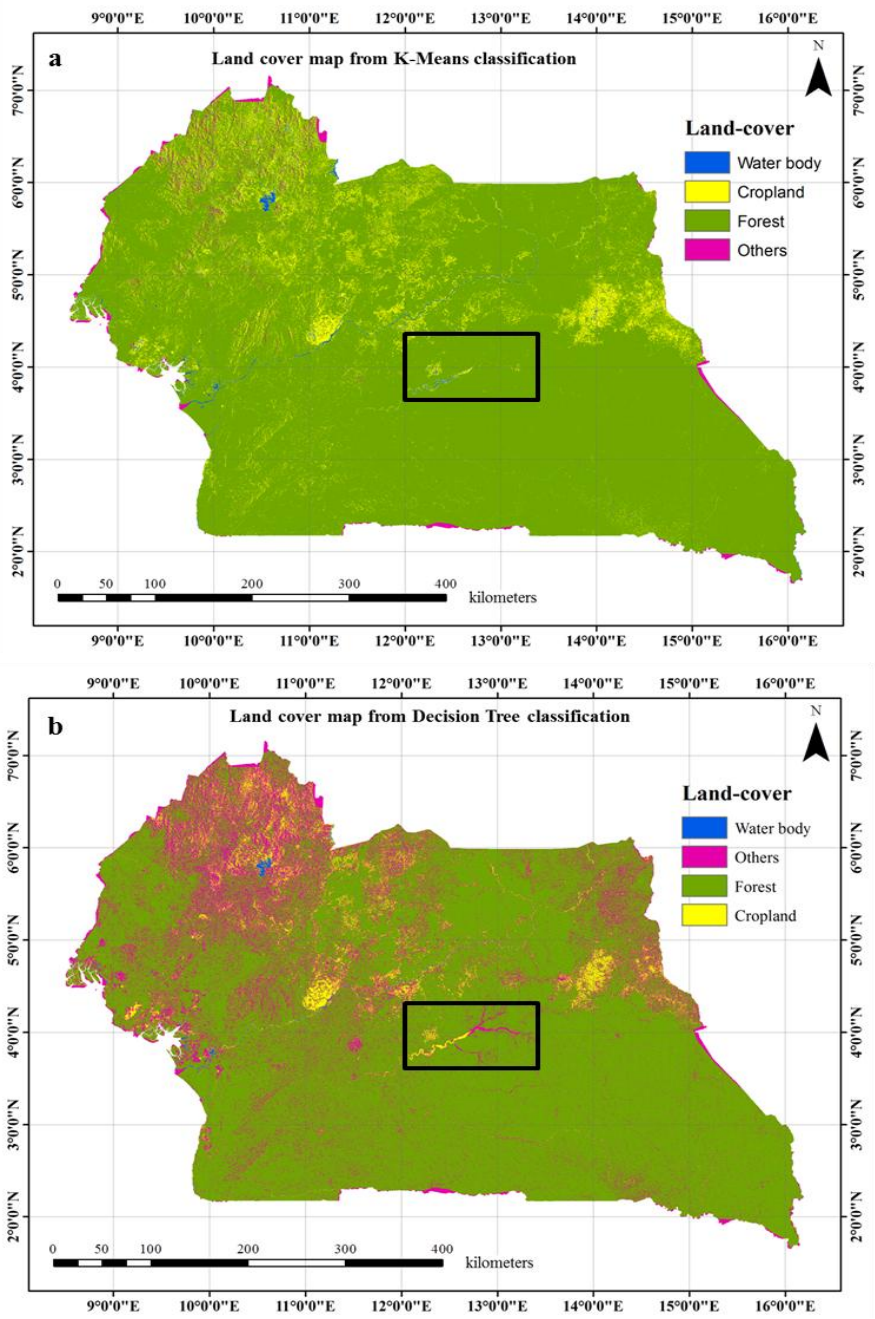

Figure 2. Land cover classes from K-means and Decision tree classifications.

We classified the spatial distribution of land cover classes in regions were ground truth data points were taken, and the analysis of three main classes; forest, water bodies and non-forest (croplands and others) is provided in Table 1 for the South, Centre and Southwest regions. Results from the different land cover classes show that there was more forest in all three regions than the other two classes. K-means classifier still estimated higher amounts of forest cover than Decision tree classifier for the South, Centre and Southwest regions approximately by 6.23 %, 10.68 % and 12.86 % respectively (Table 1). There is a higher amount of water bodies estimated by the K-means classifier than Decision tree classifier. Decision tree classifier estimated more non-forest cover than K-means classifier with a remarkable difference in all three regions (Table 1 and Figure 3). From visual inspection, it shows that K-means classifier allocated urban built-up, cocoa agro-forest, fallow lands, and plantations (tea, palms and banana) and permanently wetlands, which are near forest or far

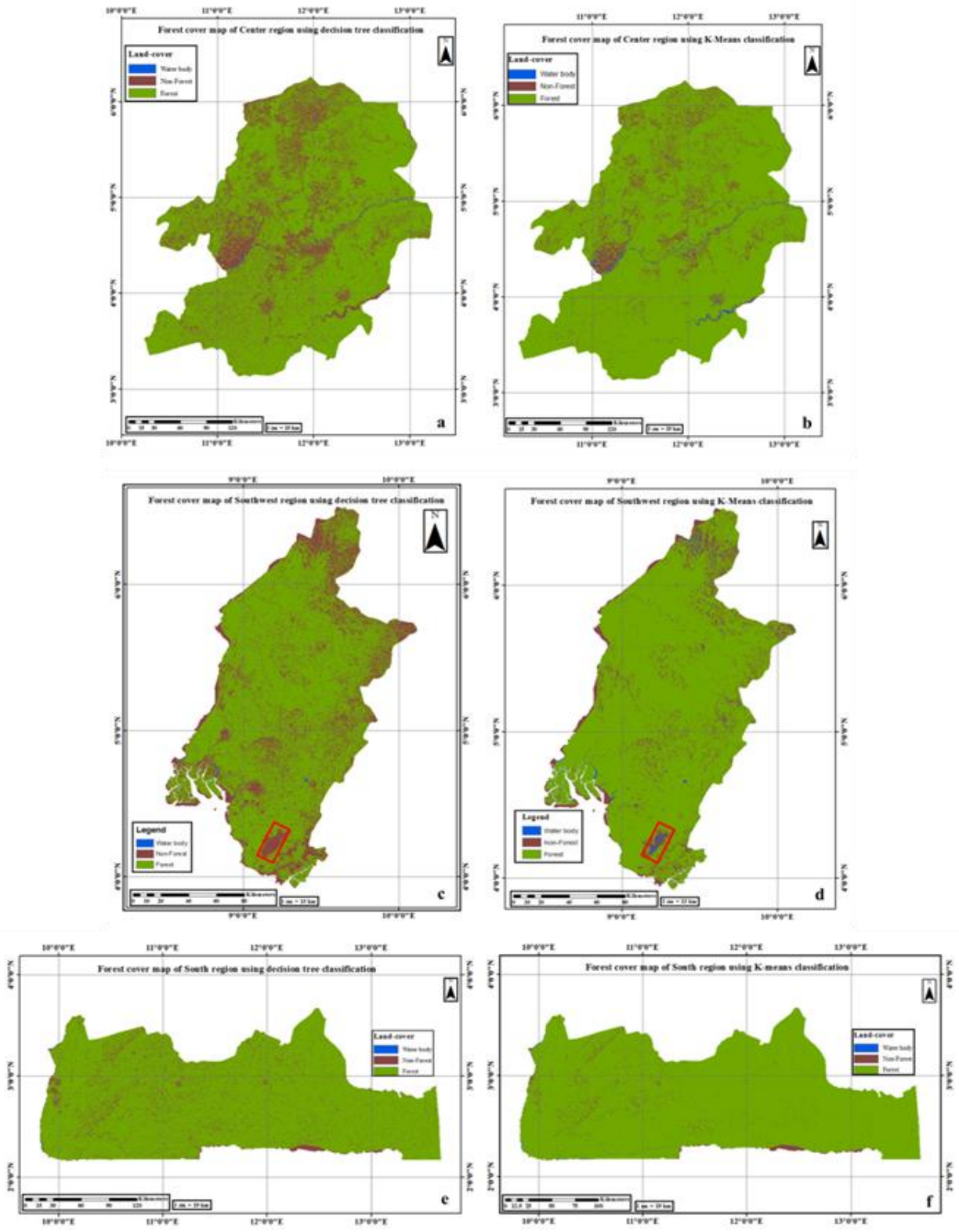

Figure 3. Land cover maps for Centre, Southwest and South regions of the Grand South where ground truth data were collected.

away from forest as forest cover class and included glacier on the mountain top to water bodies class (Figure3d). The lots of misclassifications by K-means prompted us to choose Decision tree classification to

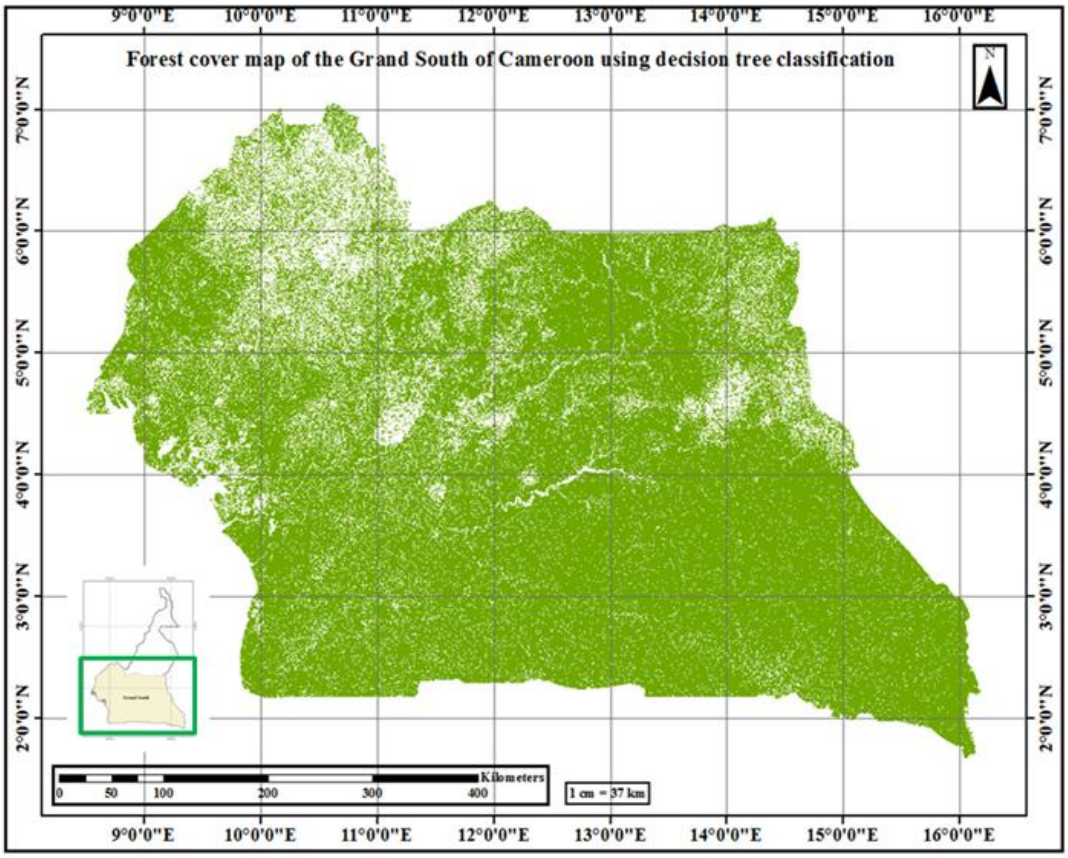

Figure 4. Forest area map for the Grand South of Cameroon demonstrating the classification details of forest cover (Green) and non-forest cover (white) based on decision tree classifier.

report forest cover estimate for the Grand South shown in Figure 4.

Accuracy Assessment of the Three Land Covers

Table 2 is the confusion matrix upon validations from the result of the decision tree classification. The confusion matrix table shows that of the 2798 pixels belonging to the forest class, the decision tree algorithm correctly allocated 2796 pixels to the forest class. And the classification algorithm incorrectly allocated 2 pixels to the non-forest class given a percentage omission error of 0.07 %. Also, 79 pixels were erroneously added to the forest class, 58 from water body and 21 from non-forest giving a 2.75 % commission error. Similarly the non-forest and the water body classes have 3.65 % and 14.97 % omission errors, respectively. The commission errors of non-forest and water body were 45.6 % and 0.09 % respectively. Finally, the overall accuracy was 91.7 % and the overall Kappa coefficient was 0.86.

Signature Analyses of PALSAR backscatter from Different Land Cover Types

Backscatter signature analyses were carried out on the three land cover types using statistical histogram analysis generated from backscatter values in HH and HV polarizations. From the histograms, average backscatter response from forest, non-forest and water bodies were calculated and it is observed that the response of forest cover in HH and HV backscatter is in the range of -11 and -2.5 dB and -16 and -6 dB respectively. The response from non-forest in HH and HV backscatter is in the range of -18.5 and -4.5 dB and -25 and -11 dB respectively. The response from water bodies in HH and HV is in the range of -24 and 0 dB and -29 and -10.5 dB respectively. From the different responses in HH and HV polarizations, it showed that there was overlapping of radar backscatter of the three classes at HH and HV (Figure 5).

To confirm the dissimilarities of backscatter responses from HH and HV we examined and visually interpreted HH and HV polarization images shown in Figure 6. There is a demarcation in backscatter between flooded area and open water bodies in HH polarization (black rectangle in HH polarization, Figure 6) and no depiction of flooded water in HV polarization (Figure 6). Thus, HH polarization is more sensitive to water bodies and flood under forest (zoom in of black rectangle in Figure 6) while HV was less sensitive to water bodies and insensitive to flood under forest. This implies HV backscattering comes predominantly from canopy scattering because there is

Table 2. Confusion matrix for the land covers classification of PALSAR 50 m orthorectified imagery in 2009 using the decision tree classifier.

	Number of ground truth pixels			
Classified pixels	Forest	Non-forest	Water body	**Total row**
Forest	2796	21	58	2875
Non-forest	2	634	529	1165
Water body	0	3	3335	3338
Total column	2798	658	3922	7378
Omission	2	24	587	
% omission	0.07	3.65	14.97	
Commission	79	531	3	
% Commission	0.09	45.6	2.75	
% Producer Accuracy	99.93	96.35	85.03	
% User Accuracy	97.25	54.42	99.91	
% Overall Accuracy	91.7			
Kappa Coefficient	0.86			
Overall match	6765			

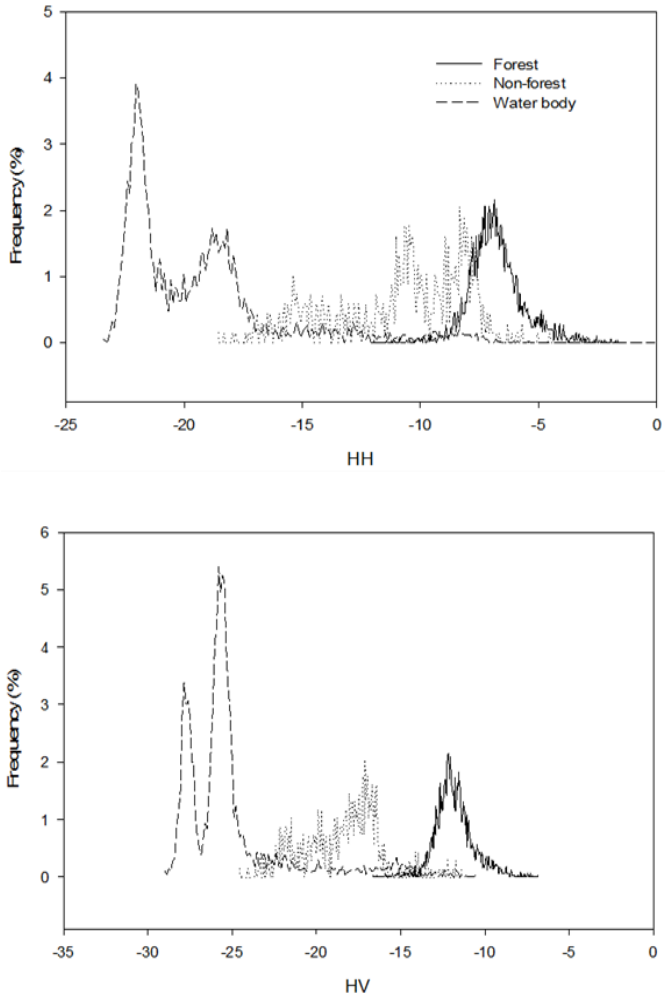

Figure 5. Backscatter histograms of land covers from HH and HV polarizations

no difference in its backscatter from flood under forest and non-flooded forest. The result is in accordance with the forest canopy scattering theory at HV backscatter (Kuga et al., 1990) and therefore HH backscatter signature is more useful in distinguishing flooded water from open water bodies, which is also in accordance with

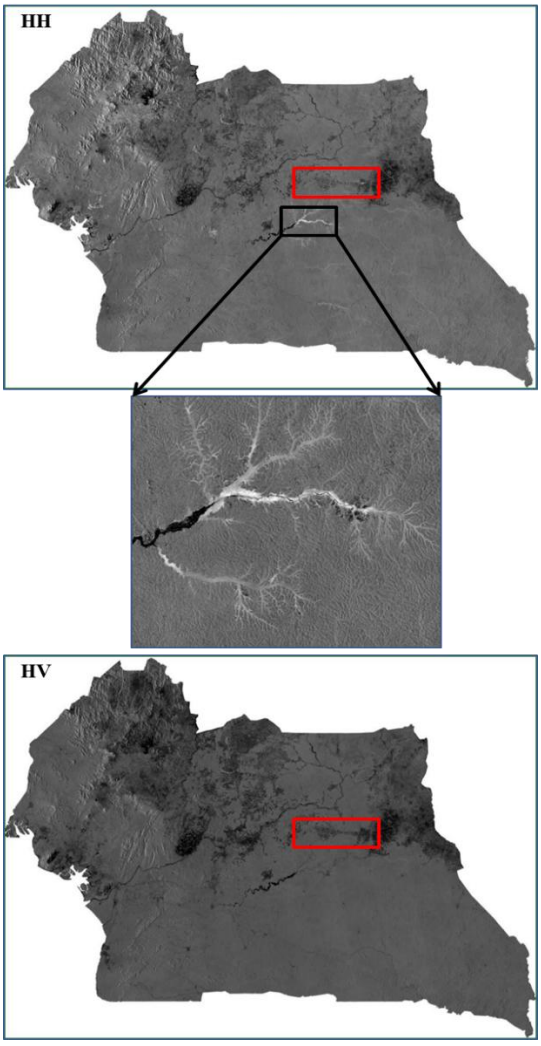

Figure 6. L-band HH and HV ALOS PALSAR mosaic images generated for the Grand South of Cameroon.

results from other studies (kasischke et al., 1997; Bourgeau-Chavez et al., 2001).

The polarization image of HH showed that total backscatter is as a result of surface-related scattering and canopy scattering. Surface-related scattering is a function of trunk-ground interactions and canopy-ground interactions and direct surface scattering. This implies that PALSAR signals interacted with the ground surface to contribute to its total backscatter while HV polarization showed that total backscattering is from direct surface scattering. Although the trunk-ground interaction was stronger in HH than in HV, it contributed less to the total backscatter in HH. From visual interpretation it shows that canopy scattering dominates in both HH and HV polarizations (Figure 6), which when modelled could be useful in validating forest cover for the study area.

We also examined the grey tone pattern in the HH and HV backscatter images of Figure 6. HH and HV backscatter show similarity in grey tones for the study area. Water bodies are clearly discriminated with a very dark grey tone due to its low backscatter (Figure 6) and this low backscatter coefficient have been reported in several studies (Chamundeeswari et al., 2007). Forest cover showed high HH and HV backscatter due to canopy reflection (the grey tone in the image) than that of water bodies (dark grey tone) while flood under forest showed bright grey tone in the HH polarization image where there is extremely high backscatter from the double-bounce between water, soil and trunk interactions (Ford et al. 1986; Waring et al. 1995) as shown in the black rectangle in HH image (Figure 6).

DISCUSSION

A comparison between the K-means and Decision Tree Classifiers

We extracted three sample regions from the Grand South (Centre, South and Southwest) for detailed comparison of K-means and Decision tree classifiers. The results from this study showed that Decision tree classifier performed better than the K-means classifier (unsupervised classification). K-means classifier showed larger amounts of water bodies and forest owing to its high level of spectral pattern recognition (Tou and Gonzalez 1974). For example, in the K-means method, glacier was included in the water body class (Figure 3d, see red rectangle) and the forest class may include other vegetation types such as palms, tea, banana plantations, and permanent wetlands and other growing crops which become very green during the rainy season, at the time which the ALOS PALSAR observation scene was covered.

The expanding population growth and population density in these regions are inextricably linked to urbanization, increase on fuel wood collection, deforestation for market-oriented agricultural land by the rich and slash and burn agriculture for income generation for smallholder farmers to meet the increasing demand for food. Decision tree classifier showed high spatial agreement with the frequent slash and burn agriculture that is heavily carried out by small-scale farmers in the regions due to the search for fertile for food security and income generation for sustainable livelihood. Though we focussed on three classes to have just the forest cover of interest, Decision tree has the ability to break complex condition of objects into simpler objects that have more homogenous samples before making a final decision (Simard et al. 2000; Lilles and et al. 2008) and is for the reason why it performed better than K-means, and was later used for the accuracy assessment for forest cover map. It is a learning algorithm that uses knowledge of individual land cover types and explores image data associated to individual land cover types. For example, for the non-forest class that included tea and banana plantations, which usually show characteristics of conti-

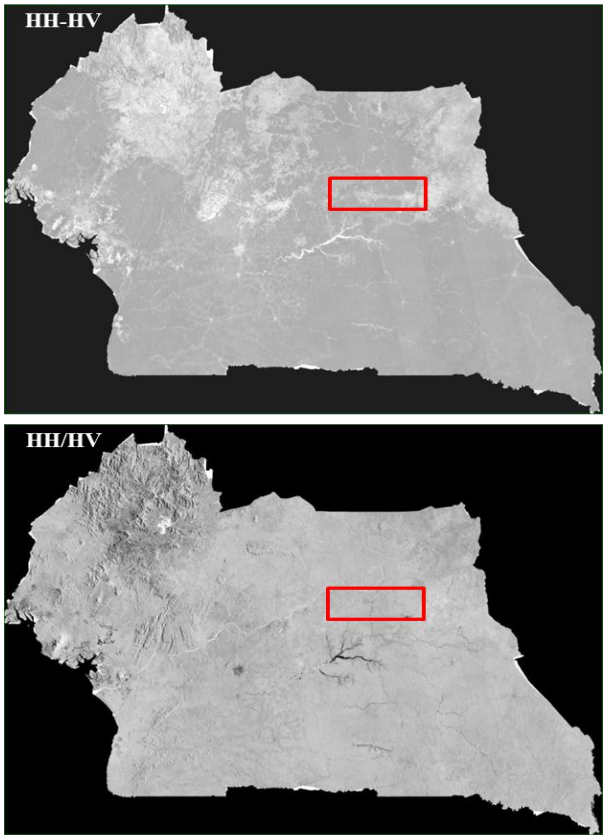

Figure 7. L-band modelled difference (HH-HV) and ratio (HH/HV) ALOS PALSAR mosaic images generated for the Grand South of Cameroon. We note the striking similar appearance of forest cover in light grey tone of HH-HV model with that of forest cover map in Figure 4.

nuous forest canopy, it was able to automatically maximize the information from the backscattering of forest cover and discarded neighbouring features that seem to relate to forest class but with less backscattering. Therefore, the forest, non-forest and water body were successfully partitioned for maximum information such that the next splits are more homogenous based on the test from each branch. Thus, it uses tree kind of method to separate classes up to simplifying what was complex to features more relevant to distinguish. Previous studies have found it appropriate for image classification using radar data because it takes advantage of backscattering and proves to be an efficient classifier to forest cover. This therefore suggests that K-means is a poor classifier for forest cover in the study area with high demographic and climatic constraints.

Potential Sources of Errors in Forest Classification

Earlier studies have used single polarization data from JERS-1 to depict clear-cuts and develop forest cover map (Simard et al. 2000) but it has been shown that single polarization-based algorithm has a deficiency to properly delineate forest cover (Miettinen and Liew 2011). This study evaluated the potential of the PALSAR fine beam dual polarization that has also been evaluated for other studies for forest delineation. The map derived from ALOS PALSAR provide reliable result not only because of the dual polarizations HH and HV, but also because of the ratio and difference modelled phase backscatter images obtained from band math in ENVI 4.8 which increase the contrast between forest cover and non-forest cover and the nature in which the shapes of the land forms appear in the study area. Backscattering signatures are very good for separability of land covers, thus, from the histograms, one could clearly see where the land covers separate from each other and where they overlap to confirm the results of the confusion matrix (Table 2). Backscatter histograms overlap in HH and HV polarizations, but the overlapping of non-forest (croplands and others) and forest classes is due to the fact that most non-forest pixels are found near forest cover. For example, farmlands of less than a hectare are established within or very close to forests. In addition, many houses in rural areas are built near the forest so reflections from roof of houses can cause considerable high radar backscatter. In addition, the image of the difference phase (Figure 7) reveals a remarkable potential of L-band ALOS PALSAR. The phase difference is based on the scattering component that contributed more to the total HH and HV backscatter. It has been shown that the phase difference of total backscatter is proportionate to dominant scattering component. For our study, the dominant scattering component for HH and HV is the canopy. Therefore the modelled phase difference is equal to the total HH and HV backscatter that mainly came from the canopy. The model phase difference is therefore similar to that of the canopy which is the forest cover. In addition, a visual comparison of the Decision tree classifier output for forest cover distribution of the Grand South (Figure 4) showed an agreeable result from the grey tone distribution of the modelled HH-HV image (Figure 7). Furthermore, the effect of canopy cover on L-band backscatter response of the study area was visually verified using field photos of the Global Geo-referenced Field Photo Library. Figure 8 is a region of the study area which is a forest/savannah transition zone. It is clear from the image tones that HH-HV clearly demarcates forest cover from non-forest covers than HH, HV and HH/HV (compare Figure 8 with Figure 9). Image texture is one of the immediate applications to support the performance of a classifier because it has a special relationship of the spatial variation in pixel intensities. (Tuceryan and Jain 1998; Champion et al. 2013). This therefore implies the use of L-band HH-HV can be used in the depiction of forest cover for this study area. However, within the forest areas, slash-and-burn agriculture are practiced and the 50-m orthorectified data must have overlooked this land cover since most of them are usually less than 50 m X 50 m, which is less than the spatial resolution of the sensor.

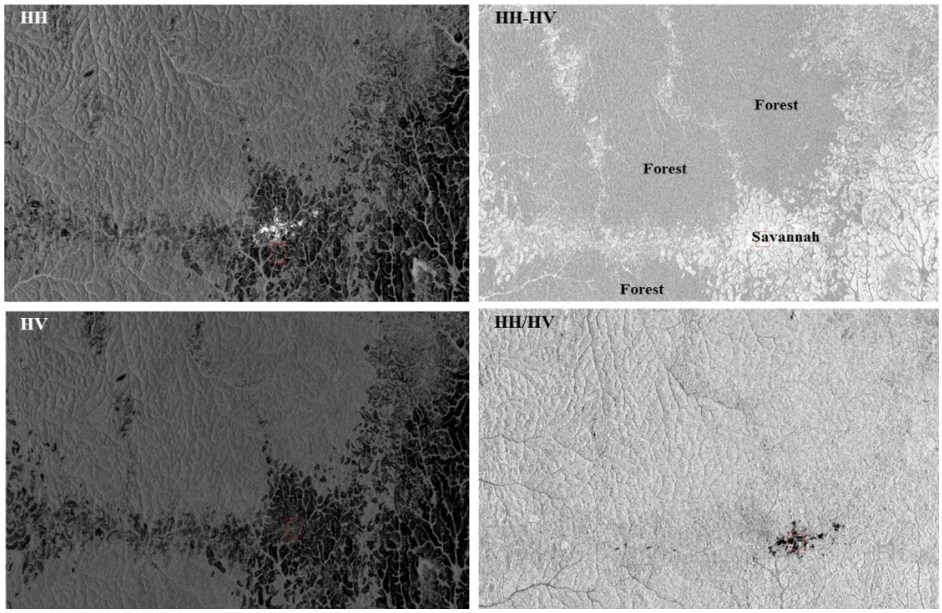

Figure 8. Part of the study area to compare reliability of results from HH, HV, the difference phase (HH-HV) and the ratio phase (HH/HV) polarizations with geo-referenced photos

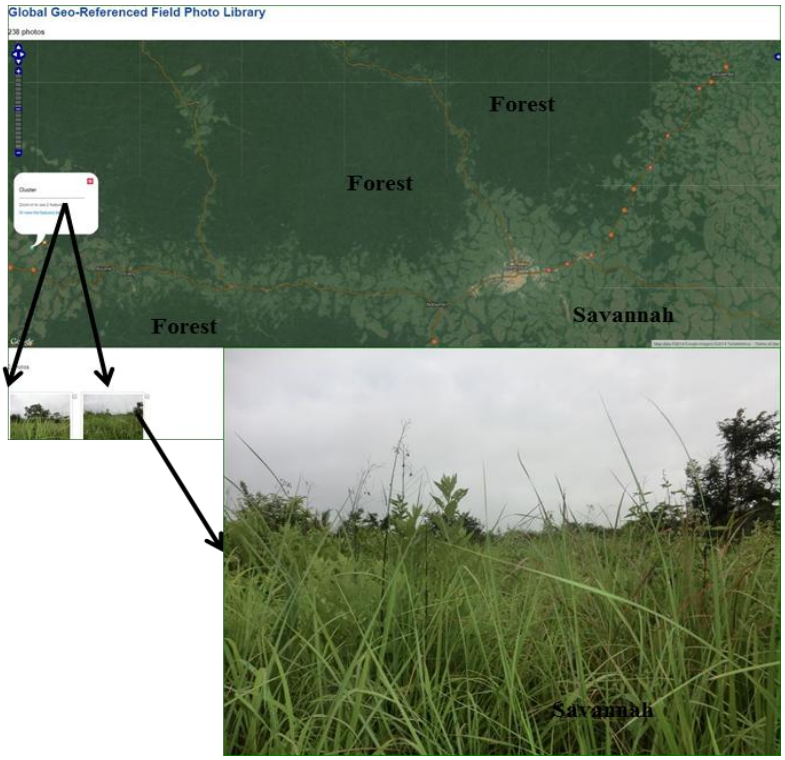

Figure 9. Part of the study area under the Global Geo-referenced Field Photo Library.

In addition, the complexity of the landscape might have also placed old fallow lands into the forest class. Therefore, small classification errors at boundaries between forest canopy/slash-and-burn agriculture/timber trails/canopy opening areas in the Decision tree algorithm might have occurred due to the 50 m spatial resolution

used in the study.

ALOS PALSAR Analysis and Validation of Forest Cover Distribution

Radar data analysis and image interpretation is usually facilitated by backscatter models most especially forest properties (van der Sanden, 1997). So, PALSAR image outputs of backscatter signatures were modelled for HH and HV polarizations using band math and Figure 7 show the modelled difference (HH-HV) and ratio (HH/HV) image of L-band backscatter intended for use in validating the spatial distribution of forest cover for the Grand South. Visually, the ratio phase displayed a perspective view of the study area in relations to hills and valleys than HH and HV, while the difference phase displayed a grey tone pattern similar to the spatial distribution of forest cover obtained by Decision tree (Figure 4) for the study area. There is a large contrast in terms of grey tones in the HH-HV image (Figure 7) to that of HH and HV polarization images (Figure 6). The very bright grey tone represents non-forest and water body classes while the forest cover is represented by the light grey tone. To confirm this, we compared side by side Figures 8 (which is the area in the red rectangle of HH, HV, and the modelled images) with that of Figure 9. Figure 9 is a particular spatial region of the study area (forest/savannah transition zone) uploaded with representative geo-referenced field photos in the Global Geo-referenced Field Photo Library to support and validate forest cover distribution by Decision tree and the difference phase of the PALSAR image. From Figure 9, the pale green area is forest cover and is equal to the light grey tone of a similar section of the HH-HV image (Figure 8) and the grey area of Figure 9 is equal to the very light grey tone of a similar section of the difference image (Figure 8). Visually, Figure 8, which is the result from the analysis using the enlarged windows of the red rectangles of Figure 6 and 7 looked promising with HH-HV window than the rest of the other windows HH, HV and HH/HV (Figure 8). This method provides information about the spatial reliability of this modelled phase to the forest distribution of the Grand South.

CONCLUSIONS

This paper introduces L–band PALSAR 50 m orthorectified mosaic imagery for mapping forest cover in the Grand South of Cameroon using Decision tree classifier. As far as we know, this is the first work that shows a 50 m spatial resolution forest cover of the Grand South derived from PALSAR orthorectified mosaic imagery. Based on our findings we estimated forest cover for the 2009 PALSAR scene to be 24.4 million hectares with an overall accuracy of 91.7 %. Our investigation showed that PALSAR imagery can be well interpreted and thus seemed to be a good sensor for forest and detection of flood under forest vegetation, which is usually difficult for other sensors to detect. In this study, a new approach for validating radar imagery using the Global Geo-referenced Field Photo Library is introduced. The method showed the importance of using geo-referenced field photos to get reliable results as to which polarizations and/or modelled backscatter image best demarcates forest cover distribution from non-forest cover. We therefore conclude that Decision tree classification performed better in the classification of land covers and the HH-HV modelled phase of the radar backscatter was the best for depicting forest cover distribution from non-forest cover.

Forest cover maps are very important for forest managers to monitor areas that are undergoing high levels of deforestation and forest degradation and guiding decision in forest resource management. Despite the great potential of ALOS PALSAR data acquisition, what is limited in this part of its Earth observation is the seasonal acquisition of data. It is recommended that continual ALOS PALSAR observation be taken over the area during the dry and rainy seasons so that data can be compared on the basis of seasons as moisture content has a lot to play on radar backscattering. It is also hoped that further studies incorporate observations from a sensor like Moderate Resolution Imaging Spectroradiometer (MODIS**)**, which has a moderate spatial resolution and very high temporal resolution to facilitate the monitoring of dynamic changes in forest cover areas (Senf et al. 2013; Dong et al. 2014).

ACKNOWLEDGEMENT

This study is supported by the National Aeronautics and Space Administration (NASA) Land Cover and Land Use Change Program (NNX11AJ35G) and the National Science Foundation (NSF) EPSCoR Program (NSF-0919466). Mr. Tenku was also supported by the Fulbright Junior Staff Development Scholarship Program. The PALSAR 50-m orthorectified mosaic imagery was provided by JAXA as the ALOS sample product.

REFERENCES

Bahuchet S (1995). History of the inhabitants of central African forests: Perspectives from comparative linguistics. In Tropical forests, People and Food. Biocultural Interactions and Applications to Development. Paris

Belward A, Lambin EF (1990). Limitations to the identification of spatial structures from AVHRR data. *Int. J. of Remote Sensing,* 5(11): 921-927.

Bourgeau-Chavez LL, Kasischke ES, Brunzell S, Mudd JP (2002). Mapping fire scars in global boreal forests

using imaging radar data, *Int. J. of Remote Sensing*, (23): 4211-4234.
Champion I, Da Costa JP, Godineau A, Ludovic V, Dubois-Fernandez P, Toan TL (2013). Canopy structure effect on SAR image texture versus forest biomass relationships. EARSeL eProceedings 12, 1/2013.
Chamundeeswari VV, Singh D, Singh K (2007). An adaptive method with integration of multi-wavelet based features for unsupervised classification of SAR images. *J. of Geophy. Eng*, 4(4): 384-393.
De Wasseige C, Devers D, de Merken P, Eba'a Atyi R, Nasi R Mayaux P (2009). Les forêts du Bassin du Congo: état des forêts 2008. EU Publications Office, Brussels, Belgium.
Devers D, Vande Weghe JP (2007). Les forêts du Bassin du Congo: état des forêts 2006. Partenariat sur les Forêts du Bassin du Congo.
Dong J, Xiao X, Chen B, Torbick N, Jin C, Zhang G, Biradar C (2014). Mapping deciduous rubber plantations through integration of PALSAR and multi-temporal Landsat imagery. *Remote Sensing of Environment*, (134): 392-402.
Epule ET, Peng C, Lepage L, Chen Z (2011). Forest Loss Triggers in Cameroon: A Quantitative Assessment Using Multiple Linear Regression Approach. *J. of Geogra. Geol.*, (3): 30-41.
Essama-Nssah B, Gockowski JJ (2000). Forest sector development in a difficult political economy: an evaluation of Cameroon's forest development and World Bank assistance. World Bank, Washington, DC.
Food and Agriculture Organization (FAO) Global Forest Resources Assessment *2010*, Rome.
Ford JP, Cimino JB, Holt B, Ruzek MR (1986). Shuttle imaging radar views the Earth from challenger. In, SIR-B Experiment. Pasadena: NASA Jet propulsion Lab.
Henderson FM, Lewis AJ (1998). Principles and Applications of Imaging Radar. Manual of remote sensing, third edition, John Wiley & Sons, New York, vol. 2, pp. xxiv + 866.
Hoyle D, Levang P (2012). Oil palm development in Cameroon. An ad hoc working paper. WWF report.
Ickowitz A (2011). Shifting cultivation and forest pressure in Cameroon. Agricultural Economics, (42): 207-220.
ITTO 2011. Country profiles. The International tropical Timber Organization.
Jensen JR (2007). Remote Sensing of the Environment: *An Earth Resource Perspective*. 2nd Ed. Upper Saddle River, NJ: Prentice Hall.
Justice C, Wilkie D, Zhang QF, Brunner J, Donoghue C (2001). Central African forests, carbon and climate change. Climate Research, (17): 229-246.
Kasischke ES, French NHF (1997). Constraints on using AVHRR composite index imagery to study patterns of vegetation cover in boreal forests. International Journal of Remote Sensing, (18): 2403-2426.
Kuga Y, Whitt MW, McDonald KC, Ulaby FT (1990). Scattering models for distributed targets, *In Radar Polarimetry for Geoscience Applications* (Ulaby FT, Elachi C Eds.), Artech House, Dedham, MA, pp. 111-190.
Laporte NT, Goetz SJ, Justice CO, Heinicke M (1998). A new land cover map of central Africa derived from multi-resolution, multi-temporal AVHRR data. *Int. J. of Remote Sensing*, (19): 3537-3550.
Letouzey R (1985). Carte Phytogeographique du Cameroun au 1/500,000. Toulouse, France.: Institut de la Carte Internationale de la Vegetation.
Lillesand TM, Kiefer RW, Chipman JW (2008). Remote sensing and image interpretation. (6th ed.). Hoboken, NJ: John Wiley and Sons.
Ling F, Li Z, Chen E, Wang Q (2009). Comparison of ALOS PALSAR RVI and Landsat TM NDVI for forest area mapping. *In IEEE 2009*, pp. 132-135.
Lucas RM, Moghaddam M, Cronin N (2004). Microwave scattering from mixed-species forests, Queensland, Australia. *IEEE Transactions on Geoscience and Remote Sensing*, (42): 2142-2159.
Mertens B, Lambin EF (2000). Land-cover-change trajectories in southern Cameroon. *Annals of the Association of American Geographers*, (90): 467-494.
Miettinen J, Liew SC (2011). Separability of insular Southeast Asian woody plantation species in the 50 m resolution ALOS PALSAR mosaic product. *Remote Sensing Letters*, (2): 299-307.
Ndoye O, Kaimowitz, D (2000). Macro-economics, markets, and the humid forest cover of Cameroon, 1967–1997. J. of Modern African Studies. *The J. of Modern Afri. Stu.* vol. 38, no. 2, pp. 225-253.
Richards T, Gallego J, Achard F (2000). Sampling for forest cover change assessment at the pan-tropical scale. *Int. J. of Remote Sensing*, 6(21): 1473-1490.
Rosenqvist A, Shimada M, Ito N, Watanabe M (2007). ALOS PALSAR: A Pathfinder mission for global-scale monitoring of the environment. *IEEE Transactions on Geoscience and Remote Sensing*, (45): 3307-3316.
Saatchi S, Soares J (1997). Mapping deforestation and land use in Amazon rainforest using SIR-C imagery. *Remote Sensing of Environment*, 2(59): 191-202.
Salas W, Ducey M, Rignot E, Skole D (2002). Assessment of JERS-1 SAR for monitoring secondary vegetation in Amazonia: II. Spatial, temporal, and radiometric considerations for operational monitoring, *Int. J. of Remote Sensing*, 7(23): 1381-1399.
Santoro M, Fransson JES, Eriksson LEB, Magnusson M, Ulander LMH, Olsson H (2009). Signatures of ALOS PALSAR L-B and Backscatter in Swedish Forest. *IEEE Transactions on Geoscience and Remote Sensing*, 12(47): 4001-4019.
Sawaya S, Haack B, Idol T, Sheoran A (2010). Land use/cover mapping with quad-polarization radar and derived texture measures near Wad Madani, Sudan. *GIScience and Remote Sensing*, 3(47): 1548-1603.
Senf C, Pflugmacher D, van der Linden S, Hostert P

(2013). Mapping Rubber Plantations and Natural Forests in Xishuangbanna (Southwest China) Using Multi-Spectral Phenological Metrics from MODIS Time Series. Remote Sens, vol. 5, pp. 2795-2812.

Simard M, Sasan S, De Grandi G (2000). The use of decision tree and multiscale texture for classification of JERS-1 SAR data over tropical forest. IEEE Transactions on Geoscience and Remote Sensing, vol. 38, no. 5, pp. 2310-2321.

Soares S, Dutra L, Perrela W (1998). Synthetic aperture radar texture classification by autoregressive modelling. Proceedings of the 2nd Latino-American Seminar on Radar Remote Sensing, Santos, Sao Paulo, Brazil, 11-12 September1998, pp. 149-151.

Tomppo E, Hallikainen M, Mikkela P, Henttonen H (1994). Application of ERS-1/SAR data in large area forest inventory. Proceedings of the First ERS-1 Pilot Project Workshop, Toledo, Spain, XX June 1994, 235-240.

Tou JT, Gonzalez RC (1974). Pattern Recognition Principles, Addison-Wesley Publishing Company, Reading, Massachusetts.

Tuceryan M, Jain AK (1998). The Handbook of Pattern Recognition and Computer Vision Chapter 2.1 by Chen, C.H., Pau, L. F. and Wang, P. S. P. (eds.), World Scientific Publishing Co, pp. 207-248.

van der Sanden JJ (1997). Radar remote sensing to support tropical forest management. Tropenbos-Guyana Series 5 Tropenbos-Guyana Programme, Georgetown, Guyana ISBN 90-5485-778-1

Walker WS, Stickler CM, Kellndorfer JM, Kirsch JM, Nepstad DC (2010). Large-Area Classification and Mapping of Forest and Land Cover in the Brazilian Amazon: A Comparative Analysis of ALOS/PALSAR and Lands at Data Sources. *IEEE Journal of Selected Topics in Applied Earth Observations and Remote Sensing*, 4(3): 594-604.

Waring RH, Way JB, Hunt ER, Morrissey L, Ranson KJ, Weishampel JF, Oren R, Franklin SE (1995). Biologists Toolbox - Imaging Radar for Ecosystem Studies. *Bioscience*, (45): 715-723.

Wilkie D, Laporte N (2001). Forest area and deforestation in Central Africa: current knowledge and future decisions. African rain forest ecology and conservation. In: Weber W. White L, Vedder A, Naughton-Treves L (eds.),. *An Interdisciplinary Perspective*, Yale University Press, New Haven, USA, pp. 119-138.

Xiao X, Dorovskoy P, Biradar C, Bridge E (2011). A library of geo-referenced photos from the field. EOS Transactions of the American Geophysical Union, 92.

Zhang QF, Devers D, Desch A, Justice CO, Townshend J (2005). Mapping tropical deforestation in Central Africa. *Environmental Monitoring and Assessment*, (101): 69-83.